Chapter 2
Description of the Test Cases

Gabriel Bugeda, Jacques Périaux, Ning Qin and Jordi Pons-Prats

Abstract The high-level objective of MARS project was to understand the formation and behaviour of turbulent structures which affects the Reynolds stress and skin friction. The aim was, once understood, to apply flow control techniques in order to control these structures and reduce the overall drag derived from the Reynolds stress and mainly from the skin friction. Active flow control devices were the main interest; DBD plasma, Synthetic jets, Micro Blowing and Suction, Moving Surfaces were included on the list. To test all these devices, two test cases were defined, and a database and file repository were established in the project webserver. The present chapter is aimed to describe the test cases, including the set-up of the flow control devices, as well as to describe the file repository were all the data was stored.

Keywords MARS · Reynolds stress · Skin friction · Drag reduction · Separation control · Flow control · DBD plasma · Synthetic jets · Blowing and suction · Slots · Synthetic Vortex Generator · Fluidric Vortex Generator · Moving Surface · Backward facing step · NACA0015

2.1 Introduction

Drag reduction and separation control are directly related to more efficient air transportation and less emission of harmful gases into the environment. While the aerospace industry is striving to have more and more optimised designs, there is still some way away from the targets set out in the ACARE 2020 vision for 50% reduction in aircraft emissions. Separation control and drag reduction contribute directly towards this target and active flow control could play an important role in achieving

G. Bugeda · J. Périaux · J. Pons-Prats (✉)
CIMNE, Barcelona, Spain
e-mail: jpons@cimne.upc.edu

G. Bugeda
Universitat Politècnica de Catalunya, Barcelona, Spain

N. Qin
University of Sheffield, Sheffield, UK

N. Qin et al. (eds.), *Advances in Effective Flow Separation Control for Aircraft Drag Reduction*, Computational Methods in Applied Sciences 52,
https://doi.org/10.1007/978-3-030-29688-9_2

it. Active flow control provides an additional dimension for further improving aircraft performance and in particular, for performance at different operational points, such as at cruise and take-off and landing.

The importance of reducing skin friction on meeting the global fuel burn targets is obvious. At cruise approximately one half of the total drag of a modern commercial transport aircraft is attributed to skin friction. The importance of improved separation control is less obvious unless we acknowledge the influence of aircraft mass on fuel burn. In fact the sensitivity of fuel burn to mass is greater than that to skin friction. Therefore if the structural mass of the aircraft can be reduced by more efficient low speed configurations or improved load alleviation off-design then this carries a significant direct benefit on cruise fuel burn.

The turbulence Reynolds stress is the most important dynamic quantity affecting the mean flow as it is responsible for a major part of the momentum transfer in the wall bounded turbulent flow. There is a lack of current understanding of the interrelationship between the various flow control devices and the Reynolds stresses in the flow field they produced. An improved understanding can potentially significantly improve the effectiveness of flow control as the Reynolds stresses are closely related to the flow behaviour at the surface for effective separation control or drag reduction. A variety of control devices are available and new ones are invented but which one for what purpose is an open question yet to be fully answered.

The focus of MARS is on the effects of a number of active flow control devices on the discrete dynamic components of the turbulent shear layers and the Reynolds stress. From the application point of view, the current proposal provides a positive and necessary step in the right direction wherein it will demonstrate the capability to control individual structures that are larger in scale and lower in frequency compared to the richness of the time and spatial scales in a turbulent boundary layer. The project will investigate active flow control means rather than passive controls.

An important characteristic of MARS project is the exploration of the possibility of influencing the mean flow via the Reynolds stress by direct manipulation of discrete structures that contribute to the stress. This is in contrast to most previous work in which the actuators change the mean flow directly. Therefore, the MARS approach offers the potential for higher system gain.

2.2 MARS Project Test Cases

Two fundamental and distinct flow cases have been chosen for the study of the effects of various flow control devices. The methodology will be based on both wind tunnel experimental investigation and numerical simulation, complementing each other for extracting flow details regarding the dynamic components and the Reynolds stresses in the shear layers, in addition to the surface properties.

The backward facing step presents a separated turbulent shear layer from a fixed sharp edge. Depending on the step height in relation to the incoming flow boundary layer thickness, various separated flow characteristics can be generated. At certain

conditions, periodic unsteady flows can be achieved and the effects of the periodic component on the turbulence Reynolds stresses can be investigated in detail. For the step flow, the reattachment zone exhibits a characteristic frequency as a function of the external fluid velocity, the flow state and the step geometry. Flow control actuators will be investigated actuators regarding their influence on the characteristic frequency, amplitude and coherence of the periodicity. The capability of the flow control on increasing and decreasing the Reynolds stresses downstream of the step will be studied. The project will also investigate whether a more responsive environment can be created for flow control.

The second basic test case is closer to a realistic wing regarding the pressure gradient but the separation from a smooth surface is more difficult to handle for unsteady flows. For the NACA0015 wing, extensive studies have been carried out with different flow control devices, including the control of training edge separation and stall characteristics. Previously, fluidic vortex generators and synthetic jets were studied for suppressing trailing edge separation and wing stall. Unsteady flow separation was observed and the responsiveness of the flow to the control input was investigated. At some flow conditions, periodicity of the dynamic components was observed. However, the detailed behaviour of the Reynolds stresses near and downstream of the control devices is not very clear so far. The project will focus on the control of the periodic component to manipulate the Reynolds stresses. The interaction of the underlying flow periodicity and the control device periodicity will be identified. For the wing case, the effects of the flow control on the Reynolds stresses can be more directly related to separation control and drag reduction.

Summarizing, the paper presents the setup of the following test cases:

– Backward Facing Step; coupled with the control devices Synthetic Vortex Generator, Synthetic Jets, Plasma and Slot
– NACA0015 coupled with Plasma, Synthetic Jets, Blowing and suction, Moving Surface and Fluidic Vortex Generators.

Regarding the optimization test cases, the ones described are:

– Backward Facing Step with Plasma and with Synthetic Jets
– NACA0015 with Synthetic Jets and with Pulsed Jets.

2.3 Backward Facing Step (BFS)

The main parameters of BFS case are shown as follow:

- Length of test section L: 4 m
- Height of test section H: 0.5 m
- Width of test section W: 0.3 m
- Height of step h: 0.01 m (adaptable)
- Location of step: 3 m from inlet of test section
- Velocity: 10–30 m/s (adaptable)

Several flow control devices can be installed on a BFS, such as SJ, movable VG, and fluid VG, etc. Some considerations for this BFS case:

A. To be separated from conventional BFS flow;
B. To get full developed turbulence;
C. To be convenience for measurements and simulations;
D. To be easy for installation of FC devices (The height of BFS can be changed).

2.3.1 Synthetic Vortex Generator (SVG)

Experimentally, the SVG consisted of a metal tape stretched over a strip of magnets placed along the span of the wind tunnel. The magnets had a width of 0.005 m and were located at 0.002 m away from the wall. AC current is applied to the metal tape generating a Lorentz force that moves the tape up and down. The frequency and magnitude of the movement is controlled by the applied current. The experimental frequency of 280 Hz produced oscillation of the strip and the amplitude was 0.002 m.

All the experimental work for this study was carried out at NUAA facilities. Figure 2.1 shows a picture of the wind-tunnel where the experiments took place.

The wind tunnel had a total height of 0.47 m and a span width of 0.30 m. The step height was 0.03 m. Experiments were carried out at a free stream velocity of 19.8 m/s and the Reynolds number based on step height was 39,000. In this case, the boundary layer thickness at step edge location was around 2H according to the experimental readings.

Fig. 2.1 Wind-tunnel facilities at Nanjing University of Aeronautics and Astronautics

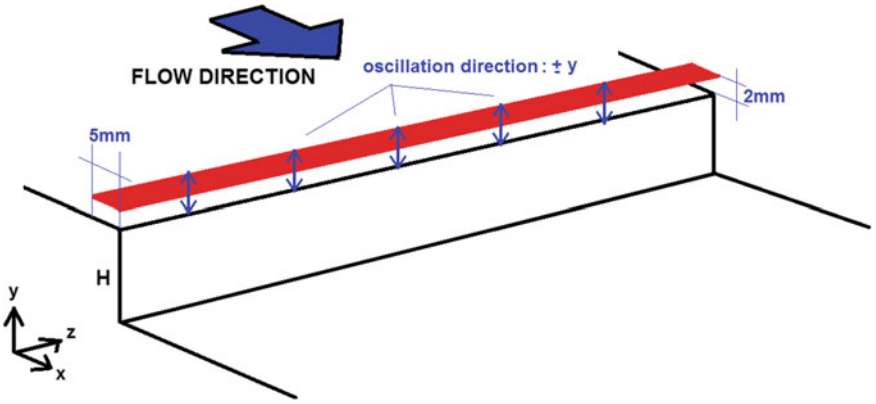

Fig. 2.2 Schematics of the simulated SVG

In order to perform the simulations, it was assumed that the SVG performed as a flat surface 0.005 m long located just before the step edge at 0.002 mm over the wall with a frequency of oscillation as the experimental, 280 Hz and maximum amplitude of 0.002 m. See Fig. 2.2.

Regarding the computational mesh, an 8 million cells provided with very reliable results. Figure 2.3 shows the computational mesh and an instantaneous capture at 0.29 s of a detail of the step region when SVG were activated in simulations.

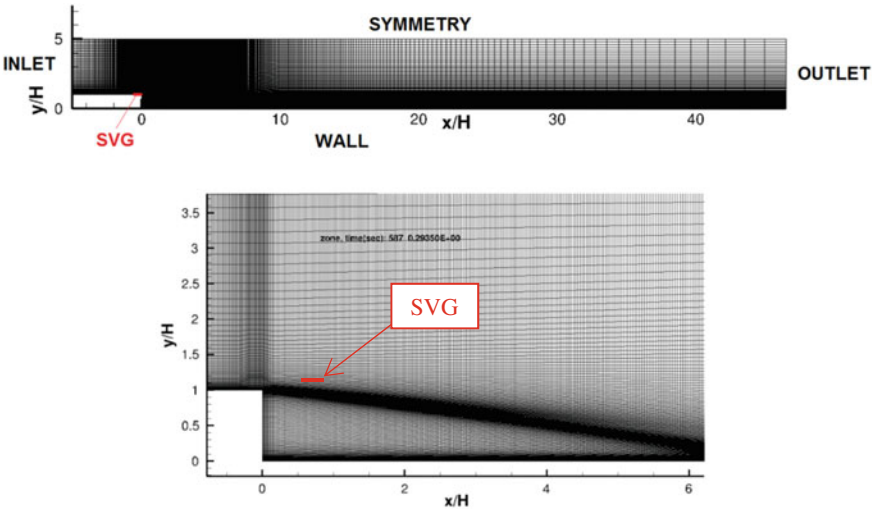

Fig. 2.3 Computational mesh and detail of step region when SVG are in operation

2.3.2 *Synthetic Jets (SJ)*

For the controlled NPU-BFS case with synthetic jets, as shown in Fig. 2.4, five jet gaps are set up in sequence along the span from the centre line and located at 65 mm upstream the step. The hole of the jets in experiment is in square shape, and distances between jets are about 40 mm. The detail parameters for this case are given in Table 2.1.

The wind tunnel in NUAA has 4 m total length, 0.5 m height and 0.3 m width. The Reynolds number is $Re_h = 8.0 \times 10^4$, based on the free-stream velocity of $U_1 = 40$ m/s and the step height h = 30 mm. On the other hand, the wind tunnel in DLR has an open test section of 0.7 m height and 1.05 m width. The Reynolds number is $Re_h = 2.0 \times 10^4$, based on the free-stream velocity of $U_2 = 10$ m/s and the step height h = 30 mm. The incoming boundary layer was artificially tripped upstream of the step to generate a turbulent boundary layer. A two-dimensional coordinate system has its origin point at the corner on the wall, a horizontal X-axis and a vertical Y-axis.

The actuator consists of a square chamber box, a thin horizontal slot, a pipe and a piston. The slot is 2 mm wide close to the step edge and facing to the downstream direction (Fig. 2.5). The square box has a cross-section of 30 × 30 mm^2. The fre-

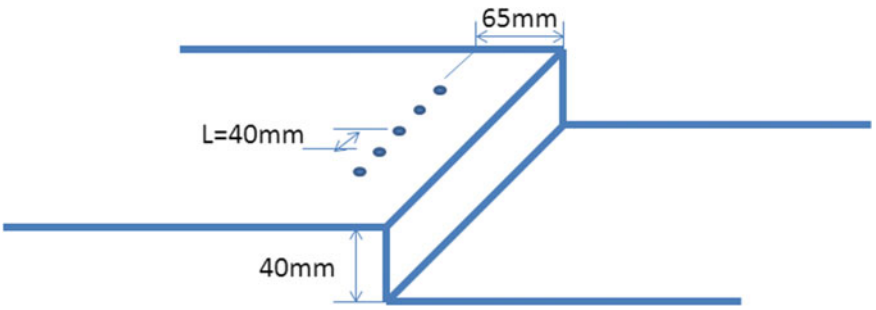

Fig. 2.4 Schematics of NPU-BFS synthetic jets test case

Table 2.1 Boundary conditions

Parameter	Value
Number of jets	5
Total span length	123 mm
Distance between jets	40 mm
Jet length	3 mm
Jet width	0.18 mm
Jet height	1 mm
Maximum jet velocity	5 m/s
Jet frequency	3000–5000 Hz
Jet density	1.17663 kg/m^3

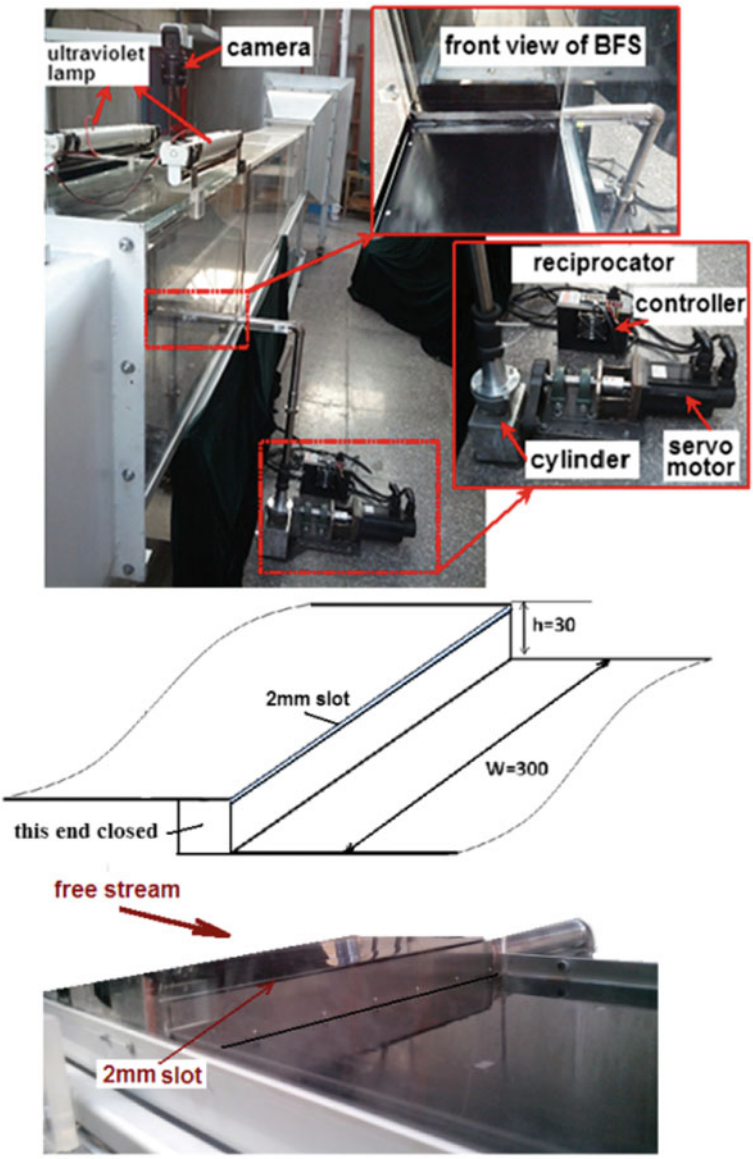

Fig. 2.5 Photo and schematic of the synthetic jet

quency of the reciprocating piston can be controlled by the servo motor. Synthetic jet is generated through the thin slot at the upper corner of the step. Three actuation frequencies of f = 0, 35 and 50 Hz were tested in NUAA by using fluorescence oil-film, while one frequency f = 100 Hz was tested in DLR by using PIV. The corresponding Strouhal number, based on the free-stream velocity and step height, are $St_h = 0$, 0.026, 0.0375 and 0.30, respectively.

2.3.3 Plasma

Experiments performed at the wind-tunnel in Poitiers facilities, Fig. 2.6, were characterised by the following configuration: the step height, H, was 0.03 m with a spanwise length of 0.3 m. The wind tunnel test section is 0.3 × 0.3 × 1. Measurements were taken at the middle section covering x/H = {−2, 7} and y/H = {−1.5, 2}.

Experiments were carried out for a free stream velocity of 15 m/s, therefore the Reynolds number based on step height is 30,000. The boundary layer thickness was calculated by means of velocity profiles measurement at various locations upstream of the step and it was determined to be approximately 13 mm at 1H before the step edge.

The actuator was mounted as shown in Fig. 2.7.

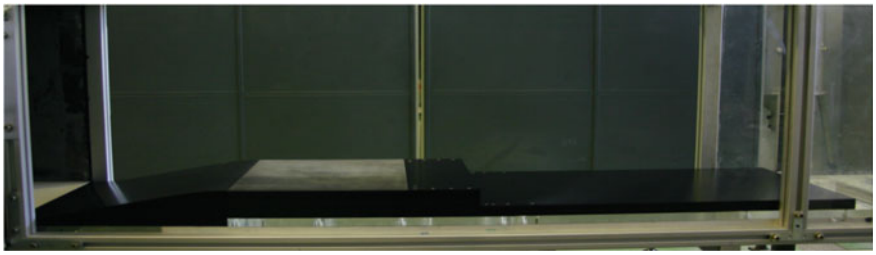

Fig. 2.6 BFS model in wind-tunnel (CNRS PPRIME Poitiers)

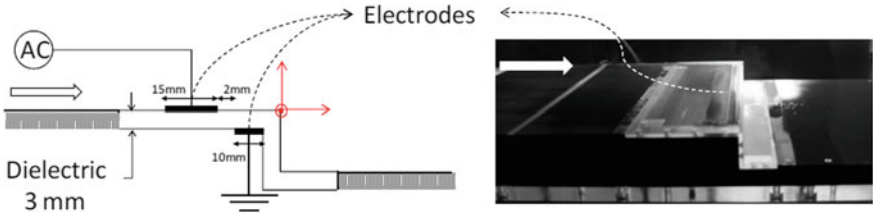

Fig. 2.7 DBD plasma actuator configuration

As it can be seen in Fig. 2.7, the exposed electrode is 0.015 m long. The embedded electrode, on the other hand, is located 0.002 m downwards the exposed and it is 0.01 m long. The dielectric thickness in this case is 0.003 mm.

2.3.4 Slot

The current simulation refers to the experiment of Driver et al. [1] in a low-speed wind tunnel, the size of whose inlet section is 1.000, 151 and 101 mm in the streamwise, spanwise and wall-normal directions, respectively. The step height, h, is 12.7 mm. The aspect ratio (the ratio of the spanwise size of wind tunnel to step height) is 12, which is large enough to ensure a quasi-2D flow in the mid-span of the wind tunnel [2]. The Reynolds number based on the free-stream velocity, $U_0 = 44.2$ m/s, and the step height, h, is $Re_h = 3.7 \times 10^4$. The boundary layer thickness is $\delta = 1.5$ h at 4 h upstream of step.

The slot harmonic actuator is located at the step edge, as shown in Fig. 2.8 with a width, d, of 0.1 h. The jet is prescribed by a velocity profile, which is uniformly distributed in spanwise direction and harmonically oscillates in time.

$$u_{ex} = U_{ex} f(\xi, \eta) \sin(2\pi f_{ex} t + \varphi)$$

where $\varphi = 0$ is the initial phase angle, f_{ex} is the excitation frequency, $U_{ex} = VRU_0$ is the amplitude and VR is velocity ratio.

The velocity profile is a laminar-like profile. An additional coefficient 1.5 is applied to ensure that the mass flow rate equal the one of the uniformly distributed profile. The profile read,

$$f(\xi, \eta) = 1.5\left[1.0 - 4.0(\xi + 0.5)^2\right]$$

where $\xi = x/d \in [-1, 0] \eta = z/d =$ x/d. The jet angle is 45° deviating from the streamwise direction.

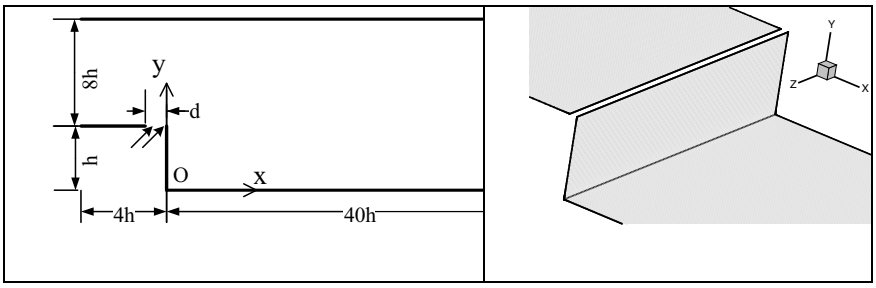

Fig. 2.8 Schematic of the slot harmonic actuator (dimensions and perspective view)

We consider the full height of the wind tunnel, which is 8 h upstream of step, so a non-slip boundary condition is applied to the upper and lower wall. The dimensions of 2D geometry are shown in Fig. 2.8. The inlet is located at x/h = −4 h, where the time-averaged velocity is available and the turbulence information is not. Hence, we conducted a 2D RANS of the wind tunnel and extracted the time-averaged velocity and turbulence information at the corresponding location to the inlet, feeding the 3D simulation. The outlet is located at x/h = 40 h, which is downstream enough to apply a convective boundary condition. Considering that the BFS flow is quasi-2D, the spanwise boundary condition is set as periodic condition. And the length of spanwise computational domain is 4 h, which is large enough to weaken the spanwise correlation [3].

2.4 NACA0015

NACA0015 geometry is well known, based on the NACA definition. It can be found on NASA archives. Following the link, a description of the geometry and aerodynamic characteristics can be found; https://ntrs.nasa.gov/archive/nasa/casi.ntrs.nasa.gov/19990047898.pdf.

2.4.1 Plasma

The experiments were conducted in one of the subsonic wind tunnels at the Aero-Physics Laboratory in the school of MACE at The University of Manchester. The facility is an open-return low subsonic 'blower' with a 0.455 m square cross section by 1.4 m long test section. The ceiling and side walls are made of optical grade perspex to allow optical access for photography and visualization. Turbulence in the test section is reduced by the presence of honeycombs located upstream of the test section. The turbulent intensity in the test section over the range of velocities used in the experiment is approximately 0.24%. The wind tunnel speed was monitored using a pitot-static tube placed upstream of the models mounted within the test section.

The aerofoil used in the experiments was a NACA0015 with a chord length, c, of 0.24 m and span of 0.40 m. For minimizing the end effects, end plates are mounted on the sides of the aerofoil made from optical grade perspex to allow visual access for ow visualization and measurements. The end plates were 0.685 × 0.457 × 0.01 m (length × height × thickness). The leading and trailing ends of the end plates were machined to have a 5 mm radius. The maximum blockage of the aerofoil which occurs at the highest incidence was estimated to be 3.9%. Therefore, tunnel blockage effect on the aerodynamic coefficients considered minimal and no correction in the measurements taken were necessary.

The configuration of plasma actuator examined in the current investigation is shown in the schematic of Fig. 2.9 [4]. The actuator is placed at the leading edge

	Width [mm]	Depth [mm]	Offset [mm]
Exposed electrode	5	0	0
A	5	0.24	0
B	40	0.48	5
C	5	0.18	45

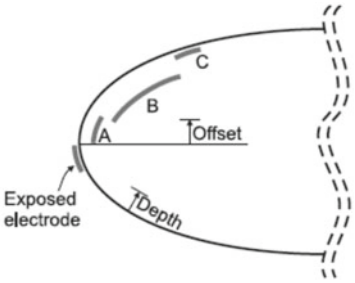

Fig. 2.9 Aerofoil actuator configuration at the leading edge (figure not scale)

while the interface of the exposed electrode and the first covered electrode is located at x/c = 0. The encapsulated electrodes are aligned so that there is no offset between the edges of successive electrodes. All the electrodes are tinned copper foils, 74 μm thick and 200 mm in length, in the spanwise direction. Layered Kapton tape was used as a dielectric material with each layer having a 60 μm thickness. Dimensions and placement of the electrodes are also provided in Fig. 2.9. The offset listed in figure is the distance measured from the downstream edge of the exposed electrode. To have a uniform plasma along the span, a small amount of overlap is applied between the downstream edge of the exposed electrode and upstream edge of the first encapsulated one.

2.4.2 Synthetic Jets (SJ)

The flow under consideration is that on a NACA0015 at $v_\infty = 10$ m/s and $\alpha = 18°$. The chord length of the airfoil is 0.5 m, and the far field boundary is 20c away from the airfoil. The width of slot is 1.5 mm, and it is located at 10%c on the upper surface of the airfoil. A structured/unstructured hybrid mesh is generated, the total number of cells is 665,000 for a 2D mesh. The airfoil is surrounded by C-type structured mesh, other part is filled by triangle mesh. There are 12 points at the slot of jet, 280 points on the upper surface totally and 120 points on the lower surface of airfoil. The corresponding 3D mesh is generated by translating the 2D mesh in span wise direction with 40 sections, and span wise length is 0.2c, as shown in Figs. 2.10 and 2.11.

On the outer boundary, the left (inlet) boundary is fixed with a uniform dimensionless inlet velocity of unity, the upper and lower boundary condition are free-stream boundaries which satisfy the Neumann condition, and the right (outer) boundary condition is set to a zero velocity gradient condition. For the airfoil, the inner boundary condition is a no-slip wall boundary condition. The near wall y^+ values of the airfoil were generally kept within 1, well within the viscous sublayer region. Three parameters (Fig. 2.12) for each jet are selected for the search investigation, namely

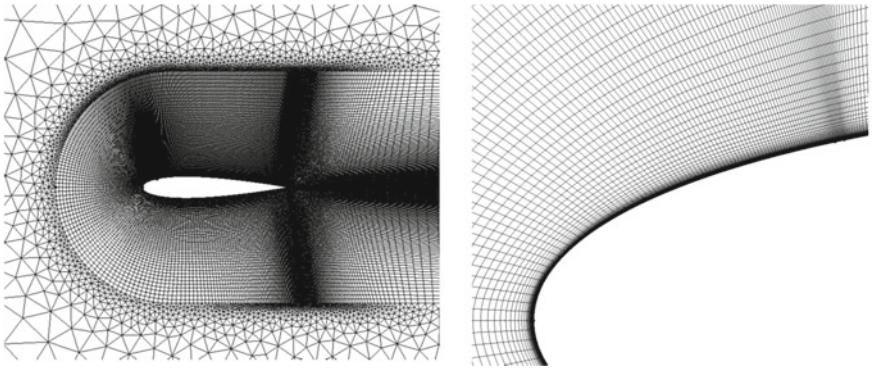

Fig. 2.10 Partial view of the mesh and mesh close to the jet

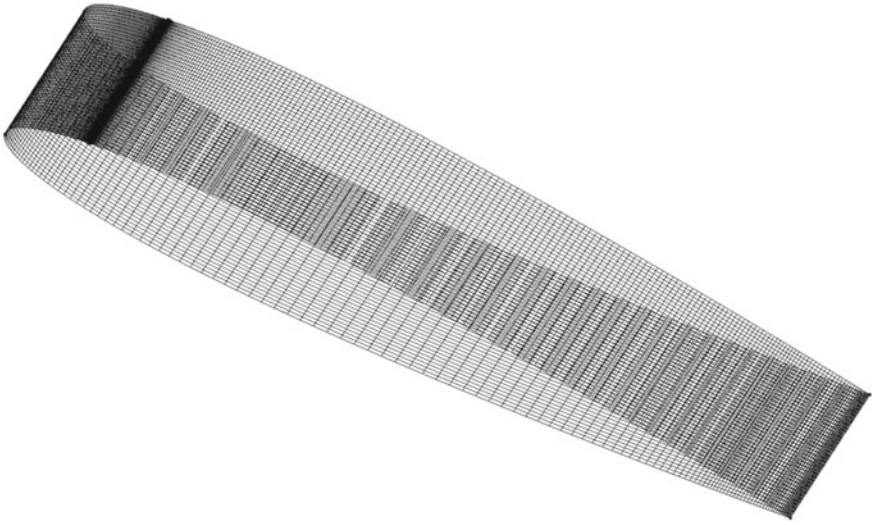

Fig. 2.11 Three dimensional mesh on the surface of wing section

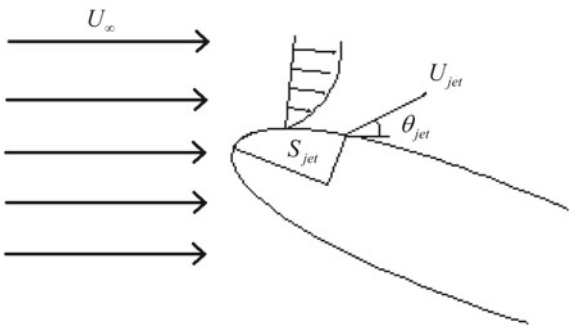

Fig. 2.12 Schematic of the jet parameters for a single jet and the baseline flow conditions

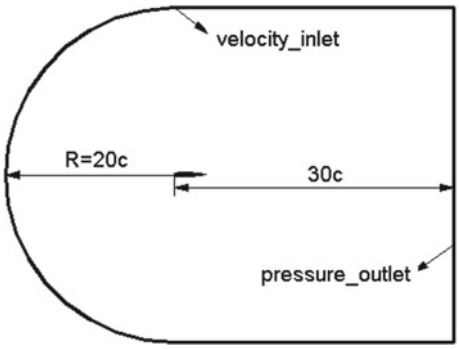

Fig. 2.13 NAC0015 airfoil computational domain

suction/blowing amplitude U_{jet}, frequency N_{jet} of jet flow and suction/blowing angle θ_{jet}. In the numerical investigation, the jet entrance velocity is set as where θ_{jet} is the angle between the chord direction and the local jet surface.

2.4.3 Blowing/Suction (MBS)

Considering a NACA0015 airfoil, the flow mechanism of separation flow control with blowing/suction approaches have been investigated. According to the experiment configuration by Giarranz et al. [5], the inflow velocity of 35 m/s and the control slots width of 0.53%c are set in present simulations, and the Reynolds number based on chord is approximate to 8.96×10^5. The flow control positions are located at 12, 30 and 70%c, respectively. The time step is $\Delta t = 5.357 \times 10^{-5}$ s, then the dimensionless time is $\Delta t^+ = 5 \times 10^{-3}$ so that every flow period is guaranteed to contain enough time steps. The flow is initialized by uniform inflow, lift and drag coefficients are averaged after a quantity of time steps with 30 iterations per time step when the periodicity of the flow is achieved.

The computational domain is shown in Fig. 2.13, the velocity inlet and pressure outlet conditions are separately utilized in inlet and outlet boundaries, while no slip wall condition is enforced on the airfoil surface.

The structured mesh used in present study contains 79,000 nodes and the airfoil surface is resolved with 472 points (Fig. 2.14). The local mesh refinements are applied near the jet location. The minimum grid size near the wall is 1×10^{-5} c, and the value of y^+ approximate to 0.3.

2.4.4 Moving Surface (MS)

A NACA0015 airfoil used in the test has a chord length 0.35 m. The MS are implemented with installation of rotating cylinders at leading edge or leeward side of the

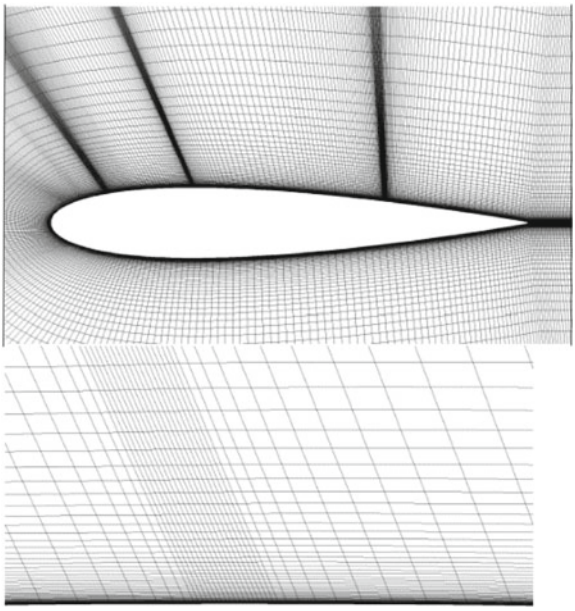

Fig. 2.14 Computational grid for NACA0015 airfoil and mesh near control device

airfoil. The front cylinder at leading edge is located at $C_1(0.05c, 0)$ with a radius $R_1 = 0.05c$, while the back cylinder at leeward side is located at $C_2(0.52c,\ 0.036c)$ with a radius $R_2 = 0.036c$. As noticed, since there are two different rotating cylinders, one can use them alone or together for boundary layer flow control. The cases include: single cylinder control at leading edge, single cylinder control at leeward side, and a combined control with cylinders at the leading edge and the leeward side both.

For the baseline case with a clean airfoil, the mesh is generated with a C-type topology, where the far field is with 50 times chord length, and a total number of volume elements about 90 thousands. The first level height from the wall is kept an order of magnitude around $10^{-6}c$. For the control cases, all meshes are generated with the same strategy and based on the baseline case to ensure a similar size and a similar distribution for all meshes (see example in Fig. 2.15).

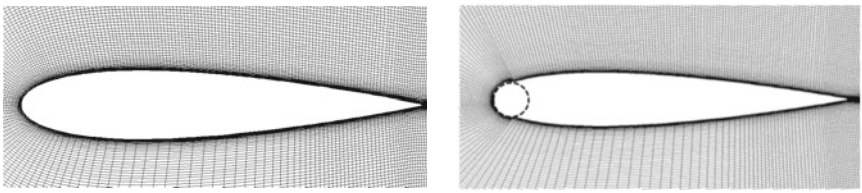

(a) clean NACA0015 airfoil (b) NACA0015 airfoil with moving surface

Fig. 2.15 Illustration of computational meshes

The flow control effect of cylinder is investigated under the flow condition at free-stream inflow velocity $U_\infty = 40$ m/s, angle of attack $\alpha = 11°$, and the Reynolds number Re/c $= 1 \times 10^6$.

2.4.5 Fluidic Vortex Generators (FVG)

NACA0015 airfoil model with a chord length of 0.35 m. We analyse the impact of the transient attachment and separation process at a Reynolds number of 1 million. To control the flow, angled fluidic vortex generators (FVG) through 44 orifices were positioned in a single array at a position of 30% from the leading edge of the airfoil.

2.5 Optimization Test Cases

2.5.1 BFS with Plasma

Backward Facing Step

The backward facing step geometry with DBD plasma actuator used in this study is modelled after the configuration in Sujar-Garrido et al. [6]. The BFS geometry and fully structured grid can be seen in Fig. 2.16. In this case, the top and bottom walls are included in the grid with a no-slip boundary condition. The inlet velocity profile applied at −10 h has been based according to experimental LDV measurements, and the velocity profile can be seen in Fig. 2.17. The 2D model has been extended in the spanwise direction by 1.4 h, with a grid resolution of 50 cells, resulting in a total cell count of approximately 4.5 million cells.

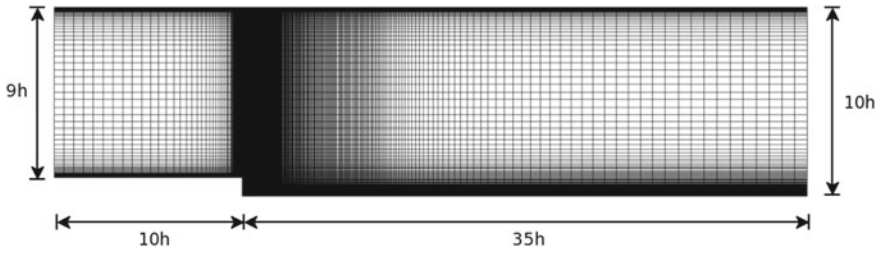

Fig. 2.16 The BFS geometry based on Súja r-Garrido et al. [6], and fully structured grid

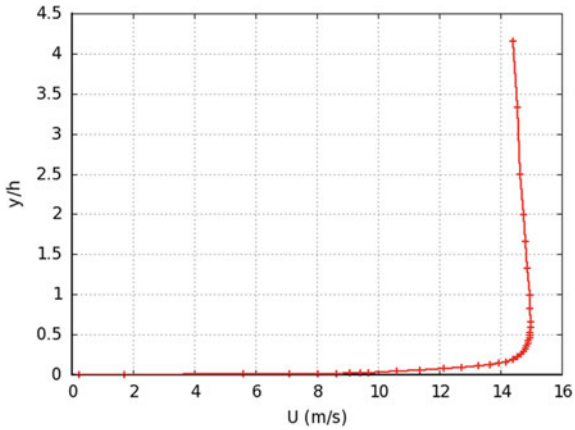

Fig. 2.17 Velocity profile at −10 h according to experimental LDV measurements by Sújar-Garrido et al. [6]

2.5.2 BFS with Synthetic Jet

Base Line Setup
The NUAA BFS wind tunnel test case

- Step height h = 30 mm
- Spanwise length = 10 h
- Wind tunnel height = 16 h before the step, the origin of the x–y axis is at the top of the step.
- Free stream velocity is 13.8 m/s.
- Reynolds number (based on h) = 30,000.
- According to experimental observations, the reattachment length is 5 h without control.

The NPU BFS wind tunnel test case

- Step height h = 40 mm
- Spanwise length = 18 h
- Wind tunnel height = 5 h before the step, the origin of the x–y axis is at the top of the step.
- Free stream velocity is 14.8 m/s.
- Reynolds number (based on h) = 40,000.
- According to experimental observations, the reattachment length is 6.5 h without control (Figs. 2.18, 2.19, 2.20, 2.21 and 2.22).

Optimisation Problem
The aim for the optimisation of the actuation is to change the Reynolds Stress distribution in the shear layer downstream the step.

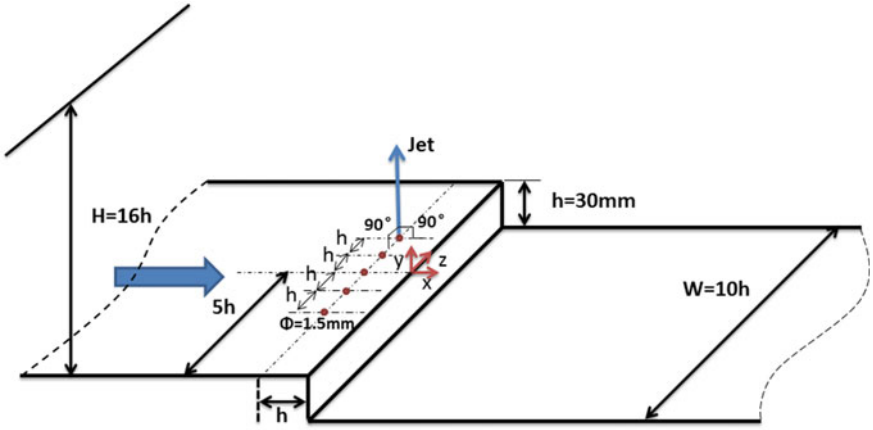

Fig. 2.18 NUAA experimental case 1

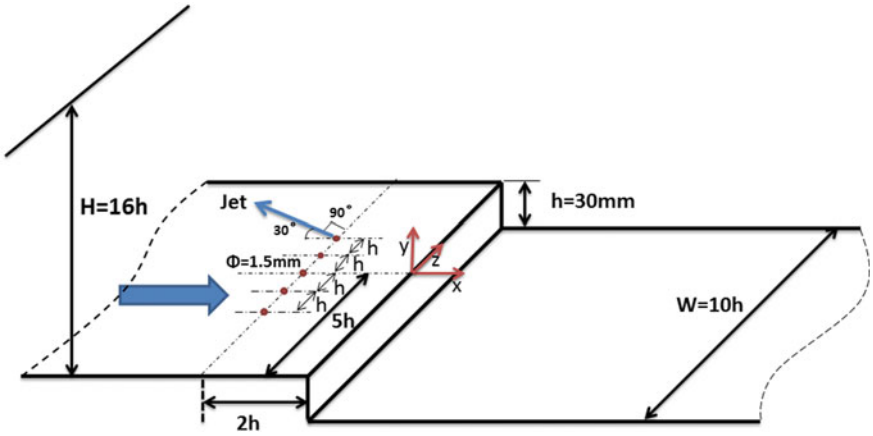

Fig. 2.19 NUAA experimental case 2

Optimization objective: The displacement of the reattached line (backward or forward).

Design Parameters

Parameter	Range
Frequency (f)	50 < f < 200 Hz
Angle of jets (based on free stream)	0°, 30°, 90°, 150°
Peak of jet velocity	3–15 m/s
Position in the stream-wise of jets	

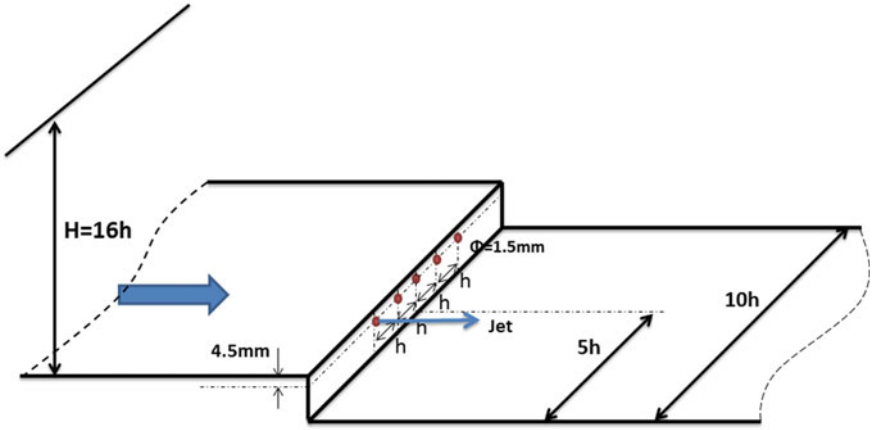

Fig. 2.20 NUAA experimental case 3

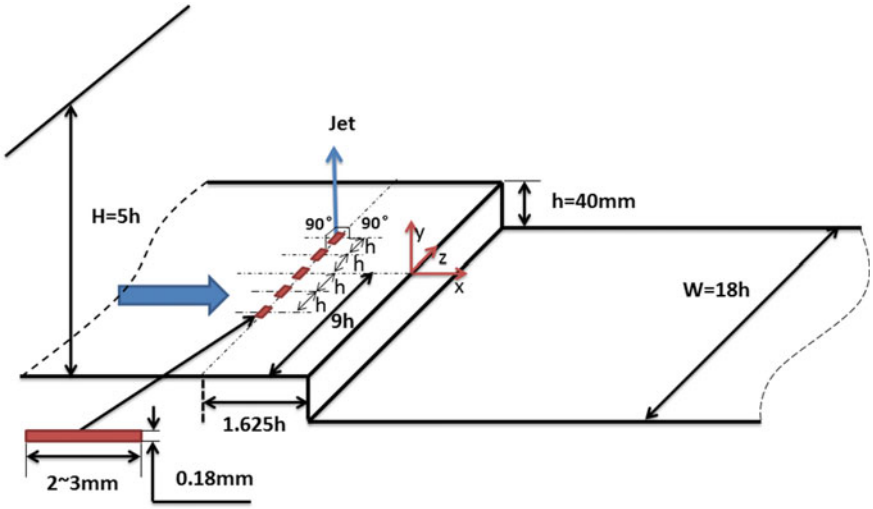

Fig. 2.21 NPU experimental case 4

2.5.3 NACA0015 with Synthetic Jet

The computational domain is defined as: upstream: 20 * C far away from leading edge, downstream: 20 * C far away from trailing edge, top boundary: 20 * C far away from chord line, bottom boundary: 20 * C far away from chord line. C is the chord length, C = 500 mm. Spanwise length = 200 mm (Fig. 2.23).

While the boundary condition; left and right boundary: periodic boundary condition, upstream, down stream, top and bottom boundary: far field boundary condition, free stream velocity = 10, 20, 30 m/s, angle of attack = 18°. No-slip boundary condition applied to the wall. Width of slot is 1.5 mm.

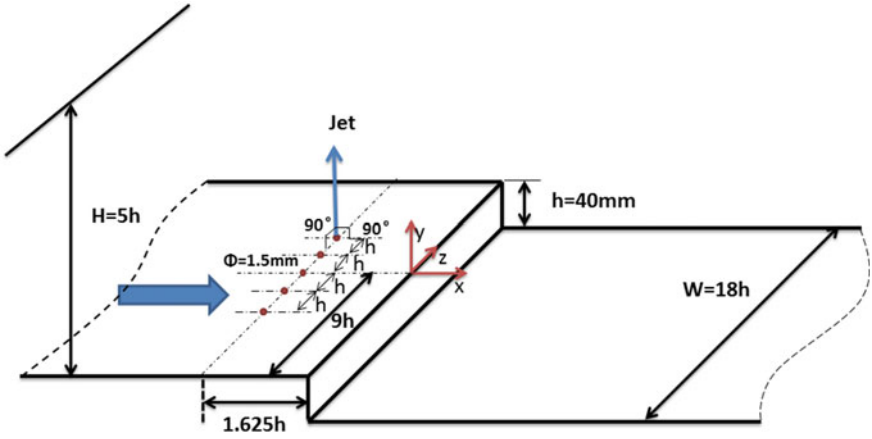

Fig. 2.22 NPU experimental case 5

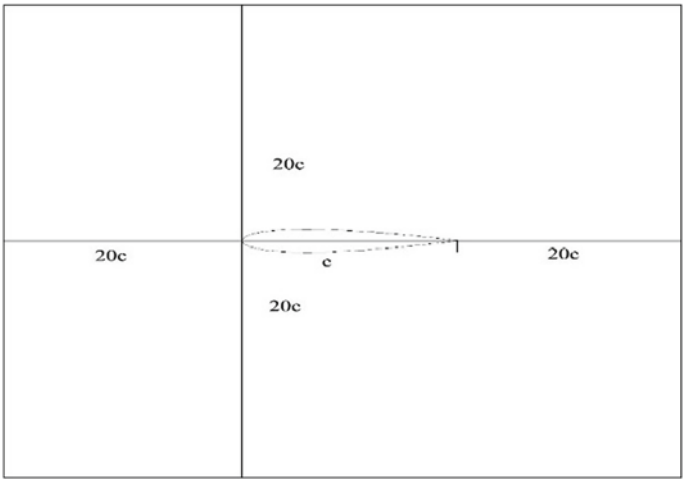

Fig. 2.23 Diagram of computational domain

The design variables are:

- frequency of jet: f, [30, 60 Hz]
- amplitude of jet flow: V_Jet, [30, 80 m/s]
- direction of jet flow: Theta, [30°, 160°]
- position of jet flow exit: p. [5–7%c].

Objective function: J is defined as the averaged lift, which should be maximized. No constraints are applied. The Optimizer is a Genetic algorithms with adaptive surrogate model.

2.5.4 NACA0015 with Pulsed Jets

Base Line Setup

The configuration of the wind tunnel and airfoil is specified in Table 2.2 and schematics with dimensional information can be seen in Figs. 2.24, 2.25 and Table 2.3.

Pulsed Jets Setup

The pulsed jets experimental configuration is described in Fig. 2.26 and Table 2.4. From Fig. 2.26 it can be seen that the orifice shape is elliptic, rather than circular. The elliptic shape of the pulsed jets can be derived from the intersection of a plane (i.e. wing surface) and a cylinder of 1 mm diameter (i.e. orifice) orientated according to Fig. 2.26. An illustration of this can be seen in Fig. 2.27.

Due to the span of the wing and number of pulsed jets, the numerical simulation has to be carried out on a smaller spanwise length to reduce computational costs. The resulting simulation model specifications that differ from the experimental configuration are listed in Table 2.5. Here, it has to be noted that the spanwise length is calculated so that periodic conditions can be correctly applied.

Table 2.2 Wing tunnel and airfoil geometric definition

Parameter	Value
Wind tunnel height	2.6 m
Wind tunnel width	2.4 m
Wind tunnel length	6 m
Aerofoil chord length (c)	0.35 m
Angle of incidence	11°

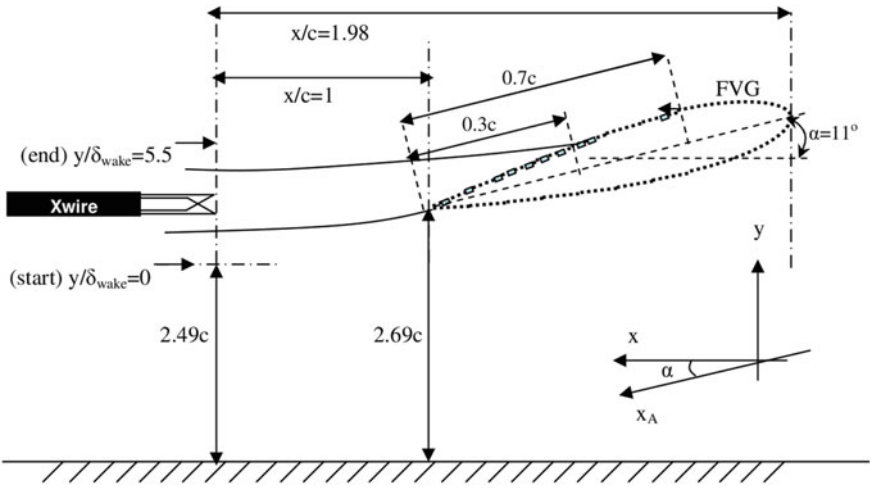

Fig. 2.24 Vertical positioning of the wing on the wind tunnel

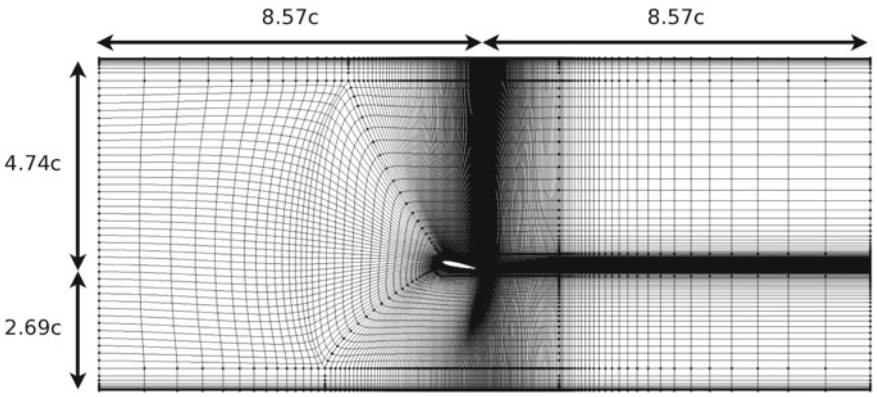

Fig. 2.25 Baseline mesh and positional information with respect to the wing's TE

Table 2.3 Boundary conditions

Parameter	Value
Velocity inlet	u = 40 m/s
Top and bottom	No slip wall
Airfoil	No slip wall
Outlet	Pressure outlet
Sides (0.2c width)	Periodic

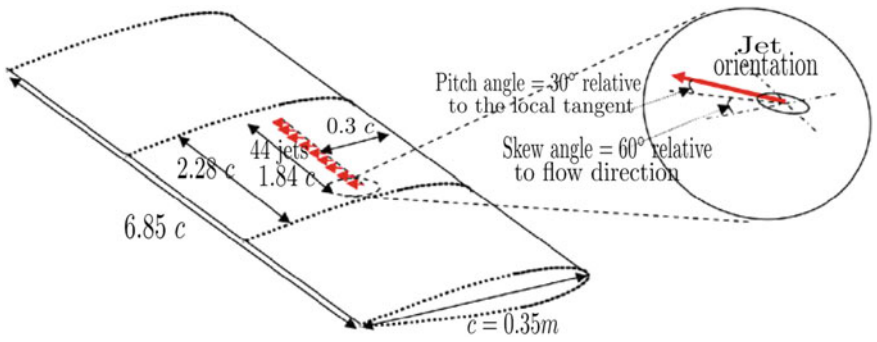

Fig. 2.26 Schematic of the pulsed jets configuration

2.5.5 Optimisation Problem

The aim for the optimisation of the pulsed jets operating parameters is to minimise the coefficient of drag C_D of the aerofoil.

The parameters for optimisation have been chosen due to their feasibility of being changed during an experimental campaign. The work duty here is defined as the

Table 2.4 Experimental fluidic vortex generators configuration

Parameter	Value
Total number of jets	44
Total span length	1.84c
Distance between jets	15 mm
Orifice diameter	1 mm
Jet velocity	200 m/s
Jet density	1.16376 kg/m^3
Pulsation frequency (on/off)	1 Hz
Work duty	50%

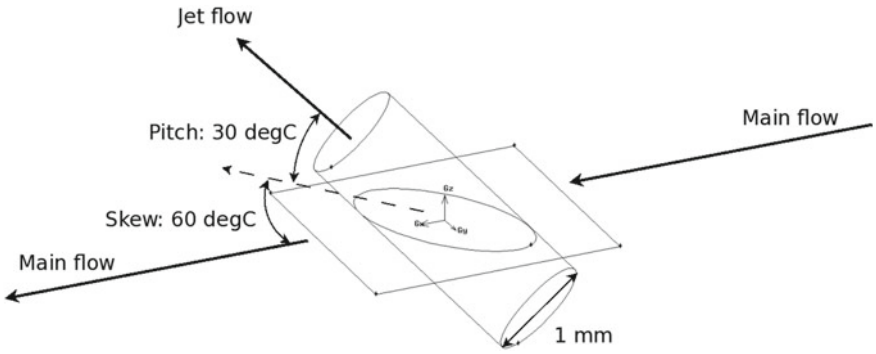

Fig. 2.27 Illustration of intersection between plane and cylinder to create the orifice elliptical shape

Table 2.5 Model parameters specific to numerical simulations

Parameter	Value
Number of FVG's	4
Span length	0.1714c
Distance between orifice centre and wing edge	0.0214c

ratio of the time where the jets are on, divided by the time for one cycle (1 Hz in the original operating parameters).

Design Parameters

Parameter	**Range**
Jet velocity, V_J	$50 < V_J < 300$ m/s
Pulsation frequency, f	$0.1 < f < 10$ Hz
Work duty, w	$20\% < w < 80\%$

2.6 Test Cases Contributors

	e——EXPERIMENTAL SIDE								WP3——NUMERICAL SIDE								
PARTNER	EU PARTNERS			CHINESE PARTNERS					EU PARTNERS					CHINESE PARTNERS			
CASE	UNIMAN	POITIER	DLR	AVIC-ARI	NUAA	BUAA	NPU		USFD	FOI	NUMECA	INRIA	CIMNE	AVIC-ARI	THU	ACTRI	BUAA
BFS			Vol PIV														
Oscillating Surfaces	X				X				X					X		X	
Plasma	X	X	X				X		X								X
Vortex Generators					X					X		X	X	X	X		
Synthetic Jets					X		X			X		X			X	X	
micro-blowing/suction					X								X				X
NACA 0015			Stereo PIV														
Oscillating Surfaces	X		X						X					X		X	
Plasma				X													X
Vortex Generators										X		X		X	X		
Synthetic Jets		X		X						X		X			X	X	
Moving Surfaces				X											X		
micro-blowing/suction						X											X

2.7 MARS website and File repository

To help communication among partners, but also to communicate the progress of the project to the general public, as part of the dissemination task within the project, a website was created. The web site was separated into two parts, a public and a private part. The private server was password protected. It was being used to assemble and distribute all project relevant information and results including agendas and minutes of meetings, reports, results and deliverables. It also includes a file repository and database to share the results of the test cases and related information.

Public Part of the MARS Web Page
The public part of the MARS web page can be found at http://www.cimne.com/mars. It contains the following sections:

- About MARS
  - Introduction
  - Objectives & Expected Results
  - Workplan
  - Consortium
- Diffusion
  - Public Docs: it contains all those documents produced by the project and considered of public access
  - Public Dissemination Activities: this is for the dissemination of the different dissemination activities organized from the project
- Members Area: this give access to the restricted part of the project file server

The first version of the web page was available in January 2011.

Restricted Part of the MARS File Server
The restricted part of the project file server contains the following sections/folders:

- Files
  - Documents
    3rd Party Publications
    Partner Publications
    Proposal and Documents
  - Project Repository
    Deliverables: here is where all files corresponding to project deliverables will be uploaded
    Meetings: here is where all documents corresponding to the different project meetings (agenda, minutes, presentations, etc.) can be uploaded.
    Technical Documents: here is where all the different working documents can be uploaded. There is a folder for each of the project tasks.

- Forum: this section allows the project participants to follow discussions about any topic related with the MARS project.
- Members: this section contains information of all participants in the project (telephone, address, photograph, e-mail, etc.). Each participant can modify and actualize his/her information when needed.
- News: this intends to be a repository of all news related with the MARS project.

All the different folders where files can be uploaded contain the corresponding self-explanatory facilities for performing the necessary operations.

Short Guide for the Website and File Repository

The website, and in particular the file repository, is organized in the most simple way. It is similar to a standard desktop environment, where folder are created to store and organize the files. The file repository was located within the MARS website (Fig. 2.28), in a private area protected with password (Fig. 2.29).

The private area of the website contains the same information as the public section, but the user can found a link to the documentation database (Fig. 2.30). The documentation is understood as the whole set of relevant data for the project and the members of the consortium. Organized under a set of folders, one can easily identify the documents related to each work package, as well as the data from each test case (Fig. 2.31). Regarding the test case folders, they were organized by test case and by contributors. In this way, all the contributors and consortium members easily located a specific data related to the test case and the contributors. The interaction between contributors were smooth and direct.

Fig. 2.28 MARS website front page and URL

Fig. 2.29 Access to the restricted area

Fig. 2.30 Access to the documentation section

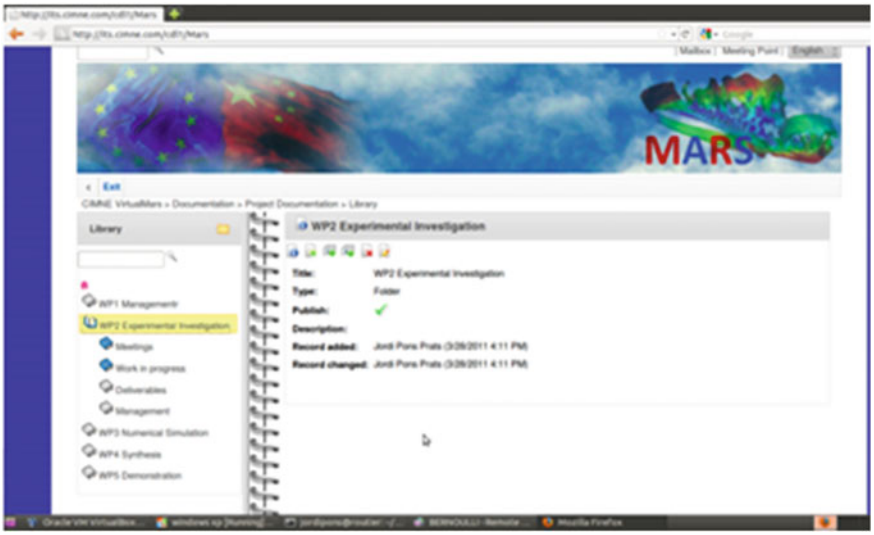

Fig. 2.31 Folders on the file repository

References

1. Driver DM, Seegmiller HL, Marvin JG (1987) Time-dependent behavior of a reattaching shear layer. AIAA J 25(7):914–919
2. De Brederode V, Bradshaw P (1972) Three-dimensional flow in nominally two-dimensional separation bubbles: flow behind a rearward-facing step. I. Department of Aeronautics, Imperial College of Science and Technology
3. Le H, Moin P, Kim J (1997) Direct numerical simulation of turbulent flow over a backward facing step. J Fluid Mech 330:349–374
4. Erfani R, Erfani T, Utyuzhnikov SV, Kontis K (2013) Optimisation of multiple encapsulated electrode plasma actuator. Aerosp Sci Technol 26(1):120–127
5. Zdravkovich MM (1997) Flow around circular cylinders: fundamentals. Oxford Science Publications. Oxford University Press
6. Sujar-Garrido P, Benard N, Moreau E, Bonnet JP (2013) Modifications of the shear layer downstream a backward facing step by dielectric barrier discharge plasma actuator. In: TSFP Digital Library Online. Begel House Inc